

## Article

# First-Principles Study of Amorphous Al<sub>2</sub>O<sub>3</sub> ALD Coating in Li-S Battery Electrode Design

Jake A. Klorman <sup>1</sup>, Qing Guo <sup>2</sup> and Kah Chun Lau <sup>1,\*</sup>

<sup>1</sup> Department of Physics and Astronomy, California State University Northridge, Northridge, Los Angeles, CA 91330, USA; jake.klorman.554@my.csun.edu

<sup>2</sup> Department of Chemistry, Washington State University, Pullman, WA 99163, USA; qing.guo@wsu.edu

\* Correspondence: kahchun.lau@csun.edu

**Abstract:** The Li-S battery is exceptionally appealing as an alternative candidate beyond Li-ion battery technology due to its promising high specific energy capacity. However, several obstacles (e.g., polysulfides' dissolution, shuttle effect, high volume expansion of cathode, etc.) remain and thus hinder the commercialization of the Li-S battery. To overcome these challenges, a fundamental study based on atomistic simulation could be very useful. In this work, a comprehensive investigation of the adsorption of electrolyte (solvent and salt) molecules, lithium sulfide, and polysulfide (Li<sub>2</sub>S<sub>x</sub> with 2 ≤ x ≤ 8) molecules on the amorphous Al<sub>2</sub>O<sub>3</sub> atomic layer deposition (ALD) surface was performed using first-principles density functional theory (DFT) calculations. The DFT results indicate that the amorphous Al<sub>2</sub>O<sub>3</sub> ALD surface is selective in chemical adsorption towards lithium sulfide and polysulfide molecules compared to electrolytes. Based on this work, it suggests that the Al<sub>2</sub>O<sub>3</sub> ALD is a promising coating material for Li-S battery electrodes to mitigate the shuttling problem of soluble polysulfides.

**Keywords:** Li-S battery; polysulfides; ALD; functional electrodes; selective adsorption



**Citation:** Klorman, J.A.; Guo, Q.; Lau, K.C. First-Principles Study of Amorphous Al<sub>2</sub>O<sub>3</sub> ALD Coating in Li-S Battery Electrode Design. *Energies* **2022**, *15*, 390. <https://doi.org/10.3390/en15010390>

Academic Editors: Almudena Benitez and Alvaro Yamil Tesio

Received: 25 November 2021

Accepted: 1 January 2022

Published: 5 January 2022

**Publisher's Note:** MDPI stays neutral with regard to jurisdictional claims in published maps and institutional affiliations.



**Copyright:** © 2022 by the authors. Licensee MDPI, Basel, Switzerland. This article is an open access article distributed under the terms and conditions of the Creative Commons Attribution (CC BY) license (<https://creativecommons.org/licenses/by/4.0/>).

## 1. Introduction

The lithium-sulfur (Li-S) battery has attracted considerable attention due to its high theoretical energy density around 2500 W · h/kg which is several times higher than that of the present commercial Li-ion batteries (LIBs) (~420 W · h/kg) [1–4]. For the Li-S battery, the overall discharge reaction can be represented as S<sub>8</sub> + 16Li<sup>+</sup> + 16e<sup>−</sup> ⇒ 8 Li<sub>2</sub>S, for which the details of the reaction pathway can be quite complicated [5]. From the reported studies, there are several intermediate polysulfide species (e.g., Li<sub>2</sub>S<sub>x</sub> with 2 ≤ x ≤ 8) formed during the discharge reaction [1,6–9]. The presence of these intermediates can be found in molecules, nanoparticles, and possibly in solid phases which were reported recently [10–13].

One of the challenges of the Li-S battery is attributed to its complicated redox processes at the sulfur cathode that results in poor cyclability. During the cycling of the Li-S battery, electrochemical reduction of elemental S<sub>8</sub> leads to the formation of soluble polysulfide species which diffuse from the sulfur cathode, and subsequently decrease the Coulombic efficiency and capacity retention of the Li-S cell [4,14,15]. Besides the capacity reduction, the crossover of polysulfide intermediates causes undesirable side reactions at the Li anode, and leads to the polysulfide shuttle [16–18]. Several attempts have been tried over the years to mitigate polysulfide dissolution, these include mechanical barriers in the sulfur cathode to inhibit polysulfides diffusion, tailored interlayers between the electrodes to prevent crossover of soluble polysulfides, additives in electrolytes to passivate the anode or control the discharge process, and the new electrolyte design to minimize the solubility of polysulfides [18–23]. These challenges are preventing the lithium-sulfur batteries from practical large-scale commercialization [24]. On the other hand, atomic layer

deposition (ALD) has been demonstrated to be a new strategy in dramatically improving the performance of lithium-ion batteries (LIBs), because of its advantages in sub-nano to nanoscale inorganic films' fabrication as a functionalized coating material [25–27]. The morphology and thickness of the ALD layer greatly depend on the coating cycles which are essential for the coating layer's function. To maintain high ionic conductivity, the ALD coatings are generally kept less than 2 nm thick on the nonmetal electrodes [28–30]. Stimulated by ALD's benefits, several works have reported utilizing the ALD to mitigate the challenges in Li-S batteries, e.g., ALD- $\text{Al}_2\text{O}_3$  on S cathodes [30], graphene-based sulfur composites [31], and nanophase S cathodes or S nanoparticles [32], etc. Besides cathodes, there have been ALD coatings (e.g.,  $\text{Al}_2\text{O}_3$ ) reported to tackle the problems associated with lithium metal anodes in Li-S batteries to mitigate the lithium metal corrosion and polysulfides' shuttling [28,33,34]. These studies have shown very promising outcomes in terms of Li-S battery cycling performance improvement due to the suppression of the polysulfides shuttle effect mainly in two aspects, i.e., adsorbents of sulfur-containing species, and/or kinetic barriers for polysulfides' dissolution [27]. However, a fundamental understanding of the electrode's interfaces, especially at atomistic scale or at molecular level, remains lacking. A systematic study with support from experiment and theory is therefore critically needed.

Inspired by these studies, we have undertaken a systematic theoretical study of the adsorption of some commonly used electrolytes' molecules (i.e., lithium bis(fluorosulfonyl)imide (LiFSI), acetonitrile (MeCN), dimethoxyethane (DME)),  $\text{Li}$ , octasulfur ( $\text{S}_8$ ), lithium sulfide ( $\text{Li}_2\text{S}$ ) and lithium polysulfide ( $\text{Li}_2\text{S}_x$  with  $2 \leq x \leq 8$ ) molecules on the amorphous  $\text{Al}_2\text{O}_3$  surface that represent the ALD- $\text{Al}_2\text{O}_3$  based on first-principles calculations. In this article, a systematic configurations exploration, based on density functional theory (DFT) to determine the low energy configurations of the molecular adsorption on the  $\text{Al}_2\text{O}_3$  surface, was performed. The low energy configurations of each adsorption system were analyzed in terms of energetics, structural, and electronic properties. With this as a baseline study, we hope we can better understand the fundamental interaction of these molecules at electrolytes/ALD-coated electrode interface during the polysulfides' dissolution process, which, in turn, will help determine whether the amorphous  $\text{Al}_2\text{O}_3$  ALD coatings can be performed as an excellent adsorbent to polysulfides.

## 2. Methodology

All the calculations were performed in the framework of DFT using the Vienna Ab Initio Simulation Package (VASP) version 5.4.4 [35,36]. The projector-augmented wave (PAW) method [37] and the Perdew–Burke–Ernzerhof (PBE) exchange–correlation functional [38] were used to describe the exchange–correlation effects. In this work, the Grimme's D3 correction term [39] was applied to include the van der Waals (vdW) interaction which was found to be substantial in Li-S systems [9,13,40]. For all the calculations, the plane-wave kinetic energy cutoff was set to 500 eV. The energy convergence was set to be  $10^{-5}$  eV, and all the configurations were fully relaxed until the residual force on each atom was less than 0.01 eV/Å. For all these DFT calculations, a  $\Gamma$ -centered K-mesh with a density of no less than 2 points per Å (i.e., KSPACING = 0.5) was used to sample the Brillouin zone during the geometry optimization. For all the simulations, the vacuum layer in the simulation cell was set to be  $\sim 15$  Å. Based on the previous experimental results [41,42], we used an amorphous  $\text{Al}_2\text{O}_3$  slab (with thickness  $\sim 8.0$  Å) to simulate the ALD coating layer. The amorphous  $\text{Al}_2\text{O}_3$  slab configuration was used in our previous work on the lithium–oxygen battery and potassium metal battery reported recently [43,44]. For each system, generally, at least three different initial configurations were considered during the geometry optimization to locate the low-energy configuration. Throughout this work, the figures related to the optimized configurations were generated using VESTA software [45].

### 3. Results and Discussion

#### 3.1. Molecular Adsorption on Amorphous Al<sub>2</sub>O<sub>3</sub> ALD Surfaces

##### 3.1.1. Electrolyte and Reactant Molecules

As shown in Figure 1, all the molecules considered in this work are found to tend to adsorb on the amorphous Al<sub>2</sub>O<sub>3</sub> ALD film when they are at close proximity to the Al<sub>2</sub>O<sub>3</sub> ALD surfaces. In Figure 1, the calculated adsorption energy is defined as:

$$E_a = -[E_{tot}(\text{system}) - (\sum_i^N E_{tot}(i) \text{ (component)})] \quad (1)$$

where  $E_{tot}(\text{system})$  and  $E_{tot}(i) \text{ (component)}$  is the total energy of the adsorbed system and individual component (e.g., Al<sub>2</sub>O<sub>3</sub> ALD slab, individual electrolyte, reactant, polysulfide molecule, etc.) predicted by DFT calculation, respectively. If the  $E_a > 0$ , then it suggests that the surface adsorption is thermodynamically feasible. The greater the  $E_a$  value, the tendency of the adsorbate molecule to bind on the Al<sub>2</sub>O<sub>3</sub> ALD surface becomes stronger. From Figure 1, a clear distinctive trend in the preferences of short- and long-chain polysulfide (i.e., Li<sub>2</sub>S<sub>x</sub> with  $2 \leq x \leq 8$ ) molecules to adsorb favorably on Al<sub>2</sub>O<sub>3</sub> ALD surface is found, compared with the electrolyte molecules. This indicates that Al<sub>2</sub>O<sub>3</sub> ALD could be used as adsorbents of polysulfides to mitigate the polysulfide shuttling in Li-S batteries which has been proved by previous experimental results [27,31,32,46].

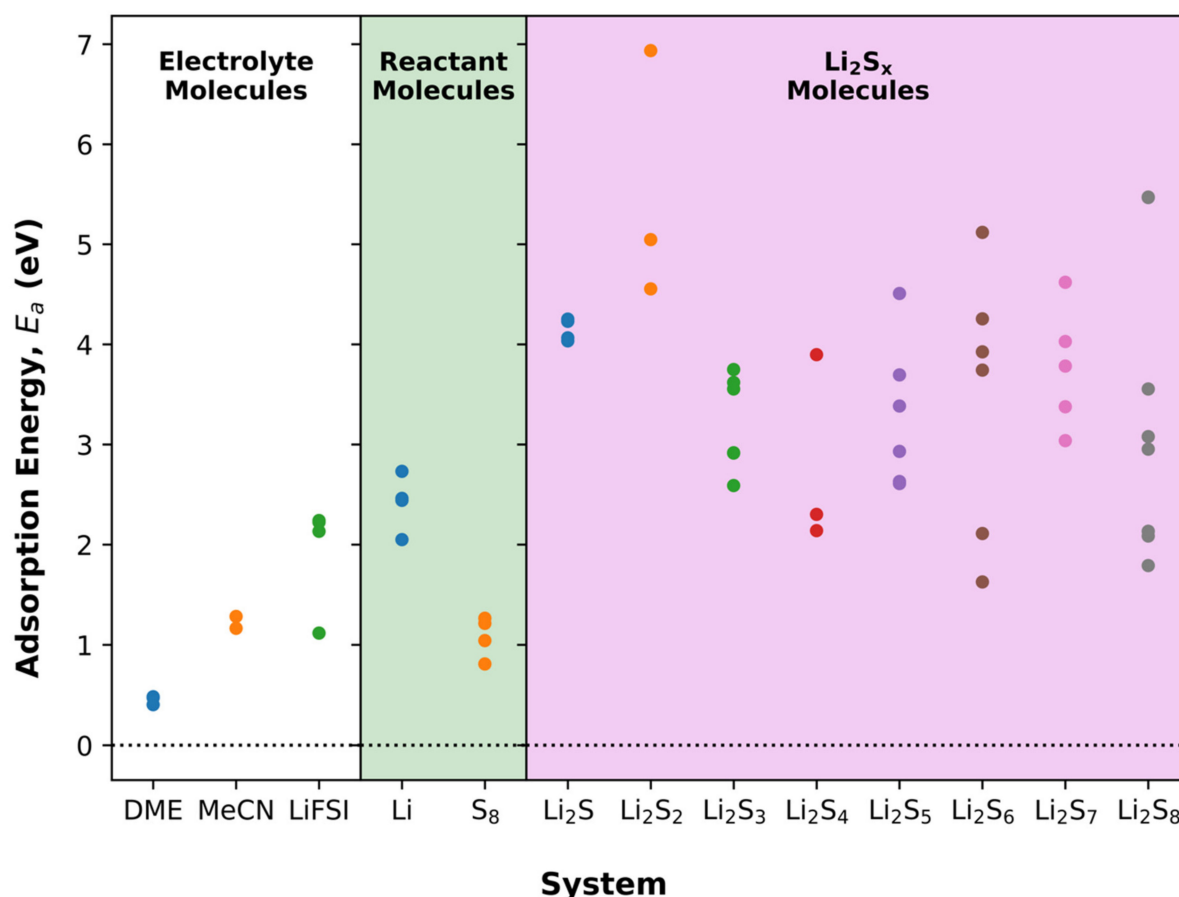


**Figure 1.** The adsorption energy,  $E_a$  (in eV) on amorphous Al<sub>2</sub>O<sub>3</sub> ALD surface of various systems that consists of electrolyte (i.e., DME, MeCN, LiFSI in the white region), reactant (Li, S<sub>8</sub> in light green region), and Li<sub>2</sub>S<sub>x</sub> with  $1 \leq x \leq 8$  (in pink region) molecules based on DFT calculations. In general,  $E_a > 0$  implies that the system is thermodynamically feasible. Each data point represents an individual configuration of geometry optimization in DFT calculations.

From DFT optimized configurations of all the systems we considered in this work, we found the interaction of solvent molecules with amorphous  $\text{Al}_2\text{O}_3$  ALD slab is considerably weaker compared to the rest. Compared to the MeCN molecule, the adsorption energy of DME molecules is generally found to be the weakest, i.e.,  $E_a \sim 0.40$  to  $0.50$  eV (Figure 1) and can be considered as physisorption on the surface (Figure 2). For MeCN molecules, the adsorption energy is  $\sim -1.15$  to  $-1.30$  eV (Figure 1), which is attributed to the strong affinity of the nitrile group to chemisorb at the aluminum sites (Al-site) on the ALD surface. For the LiFSI salt molecules, a strong tendency to bind on the  $\text{Al}_2\text{O}_3$  ALD surface is found. Compared to the solvent molecules, the energy absorption of the LiFSI salt molecule is stronger and yields  $\sim 2.24$  eV attributed to  $\text{Li}^+$  cations which bond favorably on the oxygen sites (O-site) of  $\text{Al}_2\text{O}_3$  ALD surface, besides being associated strongly with the FSI anion (Figure S1). For the configuration of dissociation of  $\text{Li}^+$  cation and FSI anion, the system is found to be equally favorable with  $E_a \sim 2.25$  eV, accompanied with a minor decomposition of FSI anion, i.e., the cleavage of S-F bond with a formation of Al-F on ALD surface (Figure S1), and this finding is consistent with the reported observation of defluorination of  $\text{FSI}^-$  anion [47] which attributed to the vulnerable S-F bonds. For the bare  $\text{Li}^+$  cations, the adsorption is found to be favorable and yields  $E_a \sim 2.73$  eV, which is even more favorable than the chemisorption of the LiFSI molecule. Whereas for the  $\text{S}_8$  molecule, it is found to only bind weakly on the ALD surface with  $E_a \sim 1.20$  eV (Figure 1), within a similar range as MeCN solvent molecules.

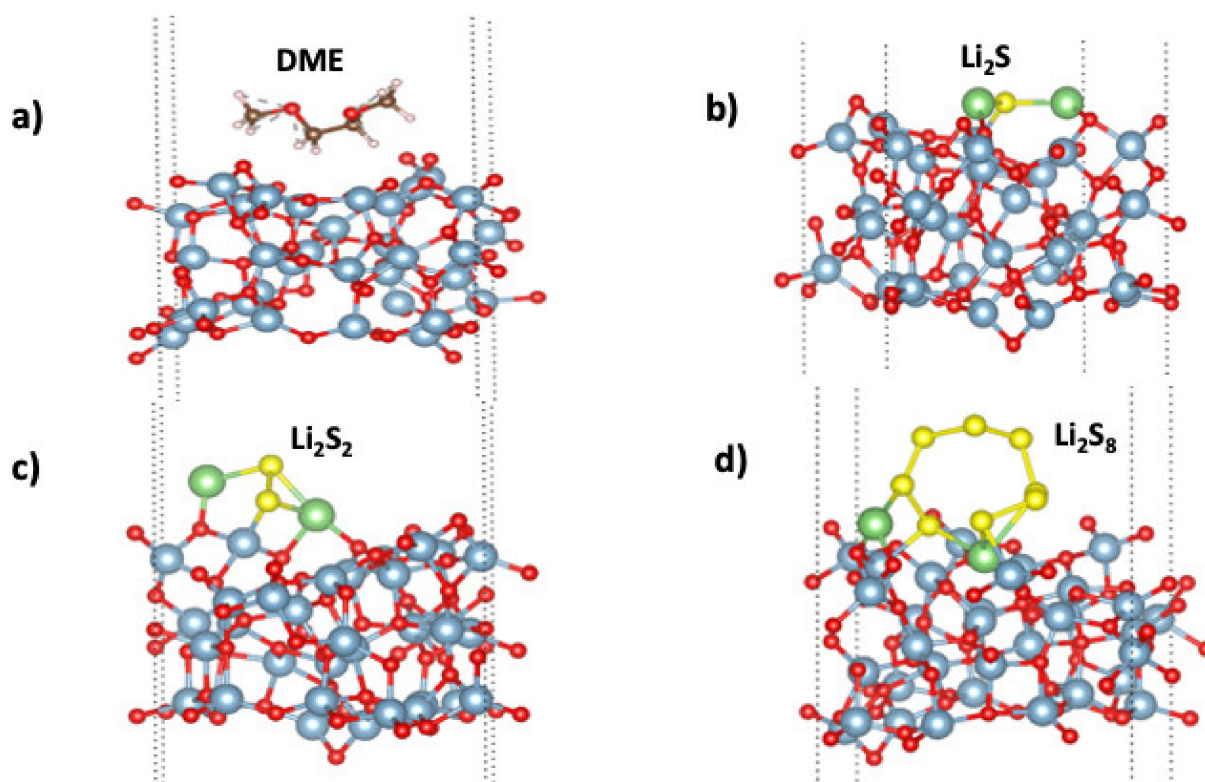


**Figure 2.** The lowest energy configuration for each system during adsorption on  $\text{Al}_2\text{O}_3$  ALD surface: (a) DME, (b)  $\text{Li}_2\text{S}$ , (c)  $\text{Li}_2\text{S}_2$ , and (d)  $\text{Li}_2\text{S}_8$  molecule. Color of atoms: oxygen (red), carbon (brown), hydrogen (white), aluminum (blue), sulfur (yellow), and lithium (green).

### 3.1.2. Lithium Sulfide and Polysulfide Molecules

Compared to the electrolytes (i.e., DME, MeCN, and LiFSI) and reactant (i.e., Li and  $\text{S}_8$ ) molecules, the  $\text{Li}_2\text{S}_x$  ( $1 \leq x \leq 8$ ) molecules are found to have a greater tendency to adsorb on the  $\text{Al}_2\text{O}_3$  ALD surfaces which dictated the considerably greater adsorption energy (Figure 1). In contrast to the DME solvent molecule, which favors physisorption on the ALD surface with at least  $\sim 2.80$  Å separation from the surface (Figure 2), the  $\text{Li}_2\text{S}_x$

( $1 \leq x \leq 8$ ) molecules are found to generally favor strong chemisorption on the ALD surface, supported by the formation of Li-O, Al-S bonds as shown in Figure 2.

Compared to the electrolytes (i.e., DME, MeCN, LiFSI) system, the adsorption energies of  $\text{Li}_2\text{S}_x$  ( $1 \leq x \leq 8$ ) molecules are substantially greater, i.e.,  $E_a > 3.0$  eV, which are usually related to the multiple bonds formation of Li-O and Al-S at the interface (Figure 2). In all cases, the spontaneous decomposition of  $\text{Li}_2\text{S}_x$  ( $1 \leq x \leq 8$ ) molecules during the adsorption process at  $\text{Al}_2\text{O}_3$  ALD surfaces are not found during the geometry optimization, which might be attributed to the strong Li-S and S-S bonds within the individual  $\text{Li}_2\text{S}_x$  ( $1 \leq x \leq 8$ ) molecules. For  $\text{Li}_2\text{S}$ , the relatively simpler molecular geometry yields several nearly degenerate chemisorbed configurations with  $E_a \sim 4.0$ – $4.2$  eV. Compared to  $\text{Li}_2\text{S}$ , a wide distribution of  $E_a \sim 2$ – $7$  eV is found for the short-chain (e.g.,  $\text{Li}_2\text{S}_x$ ,  $2 \leq x \leq 3$ ) and long-chain (e.g.,  $\text{Li}_2\text{S}_x$ ,  $4 \leq x \leq 8$ ) polysulfide molecules, which might be attributed to their relatively more complex configurations that yield various local minima during chemisorption process. For the most energetic favorable chemisorbed  $\text{Li}_2\text{S}_2$  system, the large  $E_a \sim 6.93$  eV (Figure 2) is accompanied by several bond formations of strong Li-O ( $\sim 1.80$ – $1.90$  Å) and Al-S ( $\sim 2.21$  Å), compared to the Li-O ( $\sim 1.87$ – $2.23$  Å) and Al-S ( $\sim 2.23$  Å) in  $\text{Li}_2\text{S}$  adsorption. For  $\text{Li}_2\text{S}_3$  chemisorption, the slightly fragmented  $\text{Li}_2\text{S}_3$  (i.e.,  $\text{LiS}_3 + \text{Li}$ ) molecule (Figure 3) that maximizes the formation of Li-O ( $\sim 1.79$ – $1.86$  Å) and Al-S ( $\sim 2.28$ – $2.30$  Å) bonds is found to be the most favorable with  $E_a \sim 3.75$  eV. Whereas for non-fragmented  $\text{Li}_2\text{S}_3$  chemisorption, the system is only marginally less favorable ( $E_a \sim 3.55$  eV), with longer Li-O ( $\sim 1.91$ – $2.22$  Å) and Al-S ( $\sim 2.39$ – $2.49$  Å) bonds formation on the ALD surface (Figure 3).

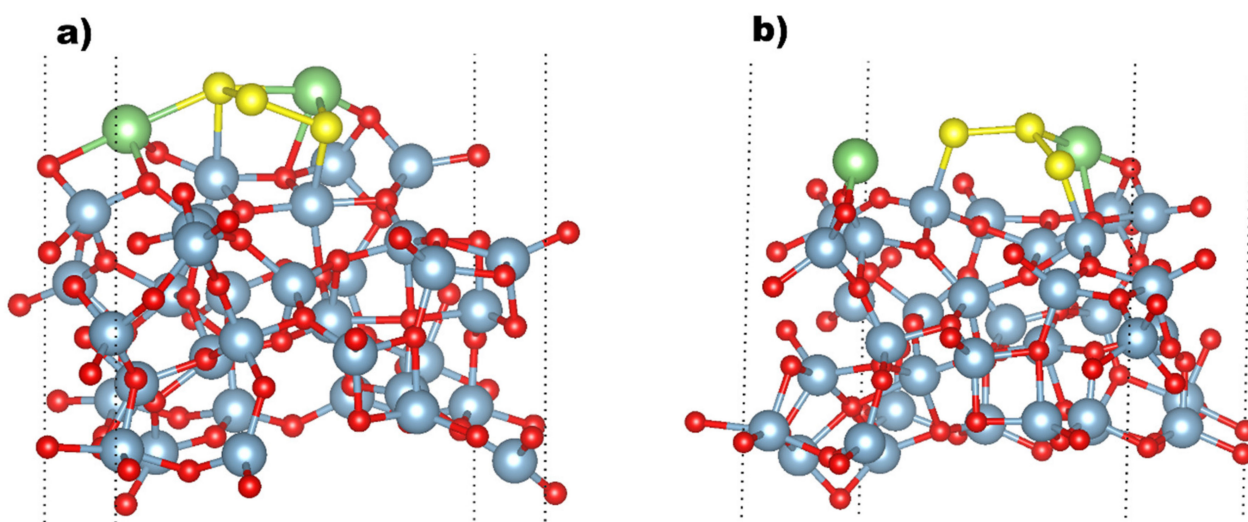


**Figure 3.** Two low energy configurations for  $\text{Li}_2\text{S}_3$  during chemisorption on  $\text{Al}_2\text{O}_3$  ALD surface. (a) The non-fragmented configuration is found with  $E_a \sim 3.55$  eV, whereas (b) is the optimized geometry which yields fragmented  $\text{Li}_2\text{S}_3$  (i.e.,  $\text{Li} + \text{LiS}_3$ ) with  $E_a \sim 3.75$  eV.

For the soluble long-chain polysulfide species which initiate the shuttle effect in Li-S battery, the considerably stronger chemisorption ( $E_a \sim 1.60$ – $5.50$  eV) (Figure 1) on  $\text{Al}_2\text{O}_3$  ALD surfaces indicates that the functionalized carbon cathode [30,32] with ALD coating might be useful in suppressing polysulfides dissolution with selective chemical adsorption when exposed to electrolytes. Compared to physisorption of DME ( $E_a \sim 0.40$ – $0.48$  eV) and weak chemisorption of MeCN ( $E_a \sim 1.15$ – $1.30$  eV) solvent molecules (Figure 1), the current DFT findings suggest that the  $\text{Al}_2\text{O}_3$  ALD surfaces can be used to trap these soluble polysulfide species to mitigate the problem caused by the shuttling of soluble polysulfide species in Li-S batteries. As highlighted in Figure 2, the most favorable configuration of  $\text{Li}_2\text{S}_8$  chemisorption ( $E_a \sim 5.47$  eV) on  $\text{Al}_2\text{O}_3$  ALD surfaces are also accompanied by the formation of Li-O ( $\sim 1.85$ – $2.10$  Å) and Al-S bonds ( $\sim 2.28$  Å) at the ALD interface, similar

to the short-chain polysulfides ( $\text{Li}_2\text{S}_x$ ,  $x = 2-3$ ) chemisorption. For the configuration of fragmented  $\text{Li}_2\text{S}_8$  during adsorption (Figure S2), the adsorption energy ( $E_a$ ) is found to be  $\sim 3.55$  eV, which indicates that fragmentation of long-chain  $\text{Li}_2\text{S}_8$  is thermodynamically less favorable during the adsorption process on  $\text{Al}_2\text{O}_3$  ALD surfaces. Interestingly, this observation is also found in other long-chain polysulfide species chemisorption, such as  $\text{Li}_2\text{S}_7$  and  $\text{Li}_2\text{S}_6$ . (Figure S2).

### 3.2. Electronic Properties

As a promising alternative to LIBs, the high energy density of Li-S batteries is attributed to lithium metal which is used as the anode. However, at current stage, the lithium metal anode has been hampered from commercialization by several technical problems, e.g., the uncontrolled lithium dendrite growth during repeated lithium extraction/deposition processes, corrosion due to lithium metal, and anode/electrolytes interfacial instability during the operating condition of Li-S batteries. As a consequence, there have been  $\text{Al}_2\text{O}_3$  ALD coatings reported for tackling these problems [28,33,34]. According to Kozen et al. [28], a uniform and conformal coating over the Li metals can be achieved based on the ALD technique to deposit ultrathin amorphous  $\text{Al}_2\text{O}_3$  coating with tunable film thickness.

From recent works [12,48], it is found that the electronic properties of short- and long-chain polysulfide solids can be quite different compared to insulating  $\text{Li}_2\text{S}$  bulk. According to DFT prediction [12,48], the polysulfide solids can be insulating or metallic depending on crystalline structures. However, the electronic properties of these polysulfides during the adsorption at the electrode interfaces remain elusive, and basic understanding remains lacking.

From the inset in Figure 3a, it is noteworthy to point out that even though it is only several atomic layers in thickness ( $\sim 8.0$  Å), the amorphous  $\text{Al}_2\text{O}_3$  ALD film is found to be insulating with an electronic bandgap  $E_g \sim 1.6$  eV according to DFT prediction (Figure S3). Thus, with an optimum thickness, it is expected that the deposition of  $\text{Al}_2\text{O}_3$  ALD coating on Li metals can provide a protecting insulating layer against the corrosion of metal anode, and further enhance the stability of anode/electrolyte interfaces. As highlighted in Figure 4, the insulating feature (i.e.,  $E_g \sim 1.5-2.0$  eV) of  $\text{Al}_2\text{O}_3$  ALD coating generally remains unchanged when exposed to physisorption and chemisorption of various adsorbates (e.g., solvent, short- and long-chain polysulfide molecules). This stability in insulating electronic properties is important and guarantees the needed stability of electrode/electrolyte interfaces in Li-S batteries' application. Regardless of whether it is physisorption or chemisorption process, the electronic density of states (DOS) attributed to the adsorbates is generally not negligible and can be considered as the surface induced electronic states close to the Fermi level ( $E_f$ ). In reminiscence of the surface-induced electronic states which are contributed by the electronic DOS of adsorbates (Figure 4), similar analogue features can also be found from the distinctive electronic charge density distribution that is present at the adsorbates/ $\text{Al}_2\text{O}_3$  ALD interfaces (Figure 5).

Compared to the weakly bound DME molecules in physisorption which exhibit a considerably delocalized character (Figure 5a), the electronic charge density distribution of adsorbates (e.g.,  $\text{Li}_2\text{S}_x$ ,  $1 \leq x \leq 8$ ) at the ALD interface are generally found to be more localized (Figure 5b-d) and can be identified as the signatures of strong Li-O and Al-S interaction on the  $\text{Al}_2\text{O}_3$  surfaces, analogous to the formation of strong Li-O and Al-S bonds during the chemisorption process (Figure 2). In all chemisorbed  $\text{Li}_2\text{S}_x$  ( $1 \leq x \leq 8$ ) systems, the presence of electronic DOS attributed to sulfur contribution at the vicinity of Fermi level is not negligible and is well-aligned to the electronic DOS of sulfur contribution at the highest occupied valence bands (HVB) from the pristine adsorbate  $\text{Li}_2\text{S}_x$  ( $1 \leq x \leq 8$ ) molecules as shown in Figure 4. Regardless of significant differences in molecular configuration, interestingly the electronic DOS of  $\text{Li}_2\text{S}_8$  chemisorption (Figure 4d) is found to exhibit similar features as  $\text{Li}_2\text{S}$  chemisorption (Figure 4b). Whereas for the physisorbed DME molecule, the dominant electronic surface states which are close to the Fermi level with oxygen contribution are attributed to carbonyl oxygen in the DME molecule and are

similar to its pristine DME molecule's electronic DOS (Figure 4a). Overall, it is evident to say that, despite some small subtle differences in local electronic DOS, the basic trend of electronic DOS of all the system during physisorption or chemisorption remain closely dictated by the electronic DOS of adsorbate molecules especially close to the Fermi level. For the electronic properties related to the influences of the possible formation of solid electrolyte interphase (SEI) which are due to the electrolytes' decomposition and lithium consumption or accumulated  $\text{Li}_2\text{S}_x$  ( $1 \leq x \leq 8$ ) layers at  $\text{Al}_2\text{O}_3$  ALD interfaces, this will be the subject of our future investigation.

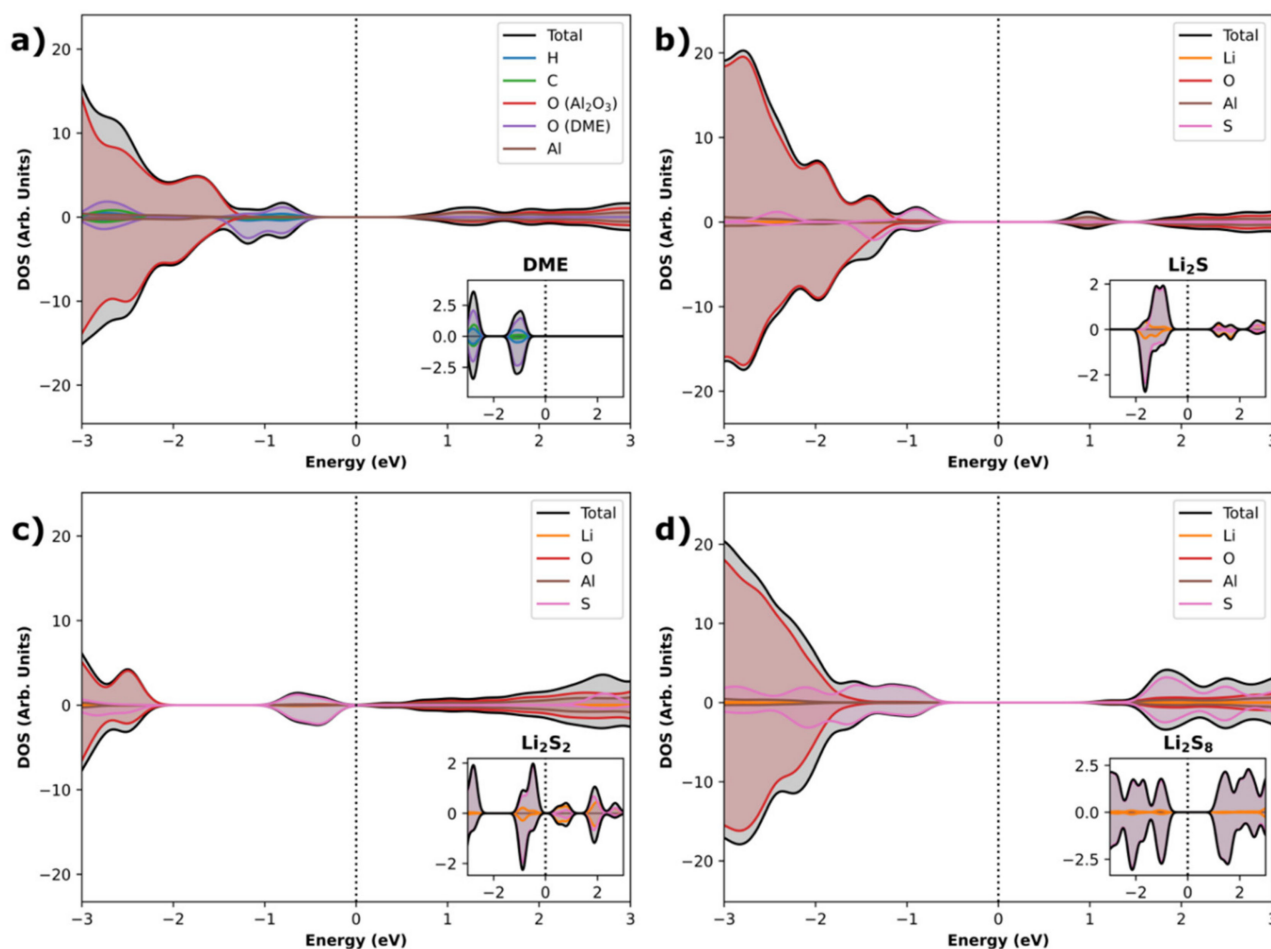


**Figure 4.** The partial electronic density of states (DOS) of the lowest energy configuration for each system during adsorption on  $\text{Al}_2\text{O}_3$  ALD surface are plotted within the vicinity of Fermi level (i.e.,  $-3.0$  eV,  $3.0$  eV): (a) DME, (b)  $\text{Li}_2\text{S}$ , (c)  $\text{Li}_2\text{S}_2$  and (d)  $\text{Li}_2\text{S}_8$  molecule. The dotted black line is the Fermi level. The total DOS, O-DOS, Al-DOS are in the black, red, and brown lines. The inset is the representative reference molecular system: the DME molecule DOS which O-DOS, C-DOS, H-DOS is in purple, green, and blue line (a: bottom right); the  $\text{Li}_2\text{S}$  molecule DOS which Li-DOS, S-DOS is in orange and pink line (b: bottom right); the  $\text{Li}_2\text{S}_2$  molecule DOS (c: bottom right) and the  $\text{Li}_2\text{S}_8$  molecule DOS (d: bottom right).

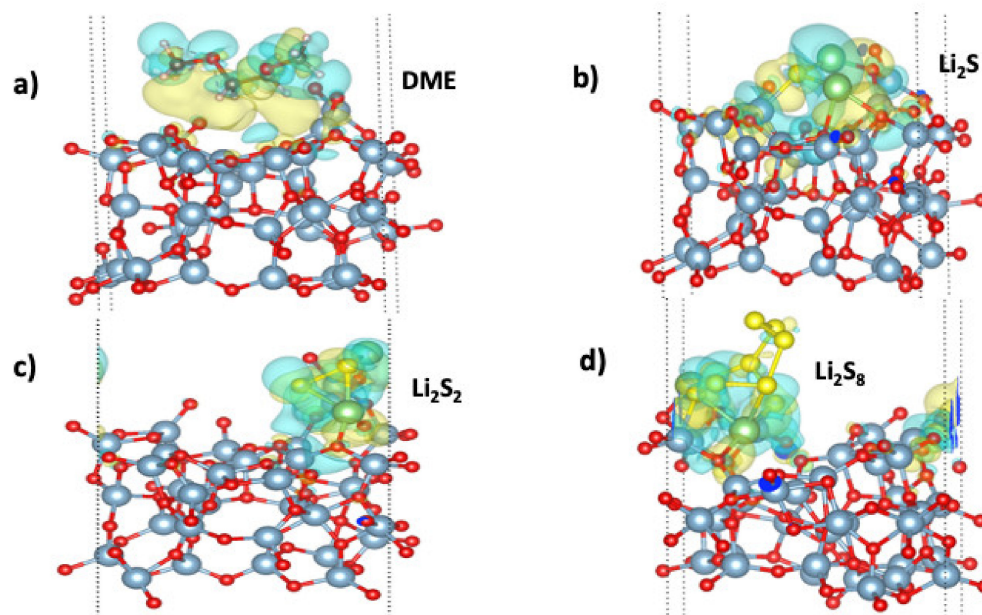


**Figure 5.** The electronic charge density difference distribution at the interface between adsorbate (a) DME, (b) Li<sub>2</sub>S, (c) Li<sub>2</sub>S<sub>2</sub>, (d) Li<sub>2</sub>S<sub>8</sub> and Al<sub>2</sub>O<sub>3</sub> ALD surface. The yellow is electronic charge accumulation (negative charge) region, while the blue is electronic charge depletion (positive charge) region. The isosurface values are  $\sim 0.001 \text{ e}/\text{\AA}^3$  with the figures generated using VESTA software [45].

#### 4. Conclusions

To obtain a basic property of amorphous Al<sub>2</sub>O<sub>3</sub> ALD surfaces when exposed to electrolytes, soluble and insoluble Li<sub>2</sub>S<sub>*x*</sub> ( $1 \leq x \leq 8$ ) molecules at electrode interfaces of Li-S batteries, we performed a systematic structural search to identify low energy configurations of various systems (i.e., DME, MeCN, LiFSI, Li, S<sub>8</sub>, and Li<sub>2</sub>S<sub>*x*</sub> with  $1 \leq x \leq 8$ ) during molecular adsorption process on Al<sub>2</sub>O<sub>3</sub> ALD surfaces using DFT calculations as our baseline study. Overall, distinguishable selective chemical adsorption of Li<sub>2</sub>S<sub>*x*</sub> (with  $1 \leq x \leq 8$ ) molecules against solvent (i.e., DME, MeCN) and LiFSI salt molecules at Al<sub>2</sub>O<sub>3</sub> ALD surfaces is found. From DFT calculations, the basic electronic properties of Al<sub>2</sub>O<sub>3</sub> ALD surfaces (i.e., electronic bandgap) remain unchanged when interacting with these adsorbates. The current DFT findings confirm the protective effects from the Al<sub>2</sub>O<sub>3</sub> ALD coating for three aspects obtained from reported experimental findings [28,30–34]: (i) acts as a kinetic barrier to decrease the direct contact between sulfur reactants and polysulfide species and the liquid electrolytes, thereby enhancing the electrodes' stability during the cell cycling, (ii) forms a quasi-envelope structure for the electrode (e.g., conducting carbon cathode) to mitigate the release of polysulfides from the electrode to the electrolyte, (iii) provides a protective layer to Li metal anodes with a more stable electrode/electrolyte interface against shuttling effects of soluble polysulfides in Li-S battery. Thus, based on the current baseline study, this indicates that Al<sub>2</sub>O<sub>3</sub> ALD coating is possibly a viable approach to fine-tune Li-S electrodes' design for the optimal performance of Li-S batteries.

**Supplementary Materials:** The following supporting information can be downloaded at: <https://www.mdpi.com/article/10.3390/en15010390/s1>, Figure S1: Two lowest energy configurations for LiFSI during adsorption on Al<sub>2</sub>O<sub>3</sub> ALD surface. (left) The Li<sup>+</sup> is associated with FSI anion during the adsorption ( $E_a \sim 2.24 \text{ eV}$ ), whereas (right) is the optimized geometry where the Li<sup>+</sup> is dissociated from FSI anion during the adsorption ( $E_a \sim 2.25 \text{ eV}$ ); Figure S2: The fragmented Li<sub>2</sub>S<sub>8</sub> (with  $E_a \sim 3.55 \text{ eV}$ , left) and Li<sub>2</sub>S<sub>7</sub> (with  $E_a \sim 4.03 \text{ eV}$ , right) during the chemisorption on Al<sub>2</sub>O<sub>3</sub> ALD surfaces; Figure S3: The electronic density of states (DOS) of pristine Al<sub>2</sub>O<sub>3</sub> ALD surfaces with band gap  $\sim 1.60 \text{ eV}$ . The black dot line is the Fermi level.

**Author Contributions:** Conceptualization, K.C.L.; methodology, J.A.K. and K.C.L.; validation, J.A.K., Q.G. and K.C.L.; formal analysis, J.A.K. and K.C.L.; investigation, J.A.K., Q.G. and K.C.L.; resources, K.C.L.; data curation, J.A.K. and K.C.L.; writing—original draft preparation, J.A.K., Q.G. and K.C.L.; writing—review and editing, Q.G. and K.C.L.; visualization, J.A.K., Q.G. and K.C.L.; supervision, K.C.L.; project administration, K.C.L.; funding acquisition, K.C.L. All authors have read and agreed to the published version of the manuscript.

**Funding:** This research was funded by Research Corporation for Science Advancement (RCSA) through a Cottrell Scholar Award (Award# 26829) and faculty start-up fund through California State University Northridge (CSUN).

**Acknowledgments:** K.C.L. acknowledges the support of the U.S. Research Corporation for Science Advancement and California State University Northridge.

**Conflicts of Interest:** The authors declare no conflict of interest.

## References

1. Bruce, P.G.; Freunberger, S.A.; Hardwick, L.J.; Tarascon, J.-M. Li-O<sub>2</sub> and Li-S Batteries with High Energy Storage. *Nat. Mater.* **2012**, *11*, 19–29. [[CrossRef](#)]
2. Peramunage, D.; Licht, S. A Solid Sulfur Cathode for Aqueous Batteries. *Science* **1993**, *261*, 1029–1032. [[CrossRef](#)]
3. Fotouhi, A.; Auger, D.J.; O'Neill, L.; Cleaver, T.; Walus, S. Lithium-Sulfur Battery Technology Readiness and Applications—A Review. *Energies* **2017**, *10*, 1937. [[CrossRef](#)]
4. Evers, S.; Nazar, L.F. New Approaches for High Energy Density Lithium-Sulfur Battery Cathodes. *Acc. Res.* **2013**, *46*, 1135–1143. [[CrossRef](#)]
5. Wild, M.; O'Neill, L.; Zhang, T.; Purkayastha, R.; Minton, G.; Marinescu, M.; Offer, G. Lithium Sulfur Batteries, a Mechanistic Review. *Energy Environ. Sci.* **2015**, *8*, 3477–3494. [[CrossRef](#)]
6. Manthiram, A.; Fu, Y.; Chung, S.-H.; Zu, C.; Su, Y.-S. Rechargeable Lithium-Sulfur Batteries. *Chem. Rev.* **2014**, *114*, 11751–11787. [[CrossRef](#)] [[PubMed](#)]
7. Yamin, H.; Gorenstein, A.; Penciner, J.; Sternberg, Y.; Peled, E. Lithium Sulfur Battery Oxidation/Reduction Mechanisms of Polysulfides in Thf Solutions. *J. Electrochem. Soc.* **1988**, *135*, 1045–1048. [[CrossRef](#)]
8. Hagen, M.; Schifffels, P.; Hammer, M.; Dörfler, S.; Tübke, J.; Hoffmann, M.; Althues, H.; Kaskel, S. In-Situ Raman Investigation of Polysulfide Formation in Li-S Cells. *J. Electrochem. Soc.* **2013**, *160*, A1205–A1214. [[CrossRef](#)]
9. Park, H.; Koh, H.S.; Siegel, D.J. First-Principles Study of Redox End Members in Lithium-Sulfur Batteries. *J. Phys. Chem. C* **2015**, *119*, 4675–4683. [[CrossRef](#)]
10. Pang, Q.; Shyamsunder, A.; Narayanan, B.; Kwok, C.Y.; Curtiss, L.A.; Nazar, L.F. Tuning the Electrolyte Network Structure to Invoke Quasi-Solid State Sulfur Conversion and Suppress Lithium Dendrite Formation in Li-S Batteries. *Nat. Energy* **2018**, *3*, 783–791. [[CrossRef](#)]
11. Li, Y.; Romero, N.A.; Lau, K.C. Structure-Property of Lithium-Sulfur Nanoparticles Via Molecular Dynamics Simulation. *ACS Appl. Mater. Interfaces* **2018**, *10*, 37575–37585. [[CrossRef](#)]
12. Guo, Q.; Lau, K.C.; Pandey, R. Novel Metallic Crystalline Phase of Li<sub>2</sub>S<sub>3</sub>. *J. Phys. Chem. C* **2019**, *123*, 28027–28034. [[CrossRef](#)]
13. Guo, Q.; Lau, K.C.; Pandey, R. A Xanes Study of Lithium Polysulfide Solids: A First-Principles Study. *Mater. Adv.* **2021**, *2*, 6403–6410. [[CrossRef](#)]
14. Yang, Y.; Zheng, G.; Cui, Y. Nanostructured Sulfur Cathodes. *Chem. Soc. Rev.* **2013**, *42*, 3018–3032. [[CrossRef](#)] [[PubMed](#)]
15. Chen, L.; Shaw, L.L. Recent Advances in Lithium-Sulfur Batteries. *J. Power Sources* **2014**, *267*, 770–783. [[CrossRef](#)]
16. Mikhaylik, Y.V.; Akridge, J.R. Polysulfide Shuttle Study in the Li/S Battery System. *J. Electrochem. Soc.* **2004**, *151*, A1969–A1976. [[CrossRef](#)]
17. Yin, Y.X.; Xin, S.; Guo, Y.G.; Wan, L.J. Lithium-Sulfur Batteries: Electrochemistry, Materials, and Prospects. *Angew. Chem. Int. Edit.* **2013**, *52*, 13186–13200. [[CrossRef](#)] [[PubMed](#)]
18. Li, X.; Banis, M.; Lushington, A.; Yang, X.; Sun, Q.; Zhao, Y.; Liu, C.; Li, Q.; Wang, B.; Xiao, W. A High-Energy Sulfur Cathode in Carbonate Electrolyte by Eliminating Polysulfides Via Solid-Phase Lithium-Sulfur Transformation. *Nat. Commun.* **2018**, *9*, 4509. [[CrossRef](#)]
19. Zhang, B.; Qin, X.; Li, G.; Gao, X. Enhancement of Long Stability of Sulfur Cathode by Encapsulating Sulfur into Micropores of Carbon Spheres. *Energy Environ. Sci.* **2010**, *3*, 1531–1537. [[CrossRef](#)]
20. Zhou, W.; Yu, Y.; Chen, H.; DiSalvo, F.J.; Abruña, H.C.D. Yolk-Shell Structure of Polyaniline-Coated Sulfur for Lithium-Sulfur Batteries. *J. Am. Chem. Soc.* **2013**, *135*, 16736–16743. [[CrossRef](#)] [[PubMed](#)]
21. Cuisinier, M.; Cabelguen, P.-E.; Evers, S.; He, G.; Kolbeck, M.; Garsuch, A.; Bolin, T.; Balasubramanian, M.; Nazar, L.F. Sulfur Speciation in Li-S Batteries Determined by Operando X-Ray Absorption Spectroscopy. *J. Phys. Chem. Lett.* **2013**, *4*, 3227–3232. [[CrossRef](#)]

22. Ma, S.; Wang, L.; Wang, Y.; Zuo, P.; He, M.; Zhang, H.; Ma, L.; Wu, T.; Yin, G. Palladium Nanocrystals-Imbedded Mesoporous Hollow Carbon Spheres with Enhanced Electrochemical Kinetics for High Performance Lithium Sulfur Batteries. *Carbon* **2019**, *143*, 878–889. [[CrossRef](#)]
23. Wu, F.; Chen, J.; Chen, R.; Wu, S.; Li, L.; Chen, S.; Zhao, T. Sulfur/Polythiophene with a Core/Shell Structure: Synthesis and Electrochemical Properties of the Cathode for Rechargeable Lithium Batteries. *J. Phys. Chem. C* **2011**, *115*, 6057–6063. [[CrossRef](#)]
24. Chen, Y.; Wang, T.; Tian, H.; Su, D.; Zhang, Q.; Wang, G. Advances in Lithium–Sulfur Batteries: From Academic Research to Commercial Viability. *Adv. Mater.* **2021**, *33*, 2003666. [[CrossRef](#)] [[PubMed](#)]
25. Meng, X.; Yang, X.Q.; Sun, X. Emerging Applications of Atomic Layer Deposition for Lithium-Ion Battery Studies. *Adv. Mater.* **2012**, *24*, 3589–3615. [[CrossRef](#)] [[PubMed](#)]
26. Meng, X. Atomic-Scale Surface Modifications and Novel Electrode Designs for High-Performance Sodium-Ion Batteries Via Atomic Layer Deposition. *J. Mater. Chem. A* **2017**, *5*, 10127–10149. [[CrossRef](#)]
27. Sun, Q.; Lau, K.C.; Geng, D.; Meng, X. Atomic and Molecular Layer Deposition for Superior Lithium-Sulfur Batteries: Strategies, Performance, and Mechanisms. *Batter. Supercaps* **2018**, *1*, 41–68. [[CrossRef](#)]
28. Kozen, A.C.; Lin, C.-F.; Pearse, A.J.; Schroeder, M.A.; Han, X.; Hu, L.; Lee, S.-B.; Rubloff, G.W.; Noked, M. Next-Generation Lithium Metal Anode Engineering Via Atomic Layer Deposition. *ACS Nano* **2015**, *9*, 5884–5892. [[CrossRef](#)]
29. Lee, J.-T.; Wang, F.-M.; Cheng, C.-S.; Li, C.-C.; Lin, C.-H. Low-Temperature Atomic Layer Deposited Al<sub>2</sub>O<sub>3</sub> Thin Film on Layer Structure Cathode for Enhanced Cycleability in Lithium-Ion Batteries. *Electrochim. Acta* **2010**, *55*, 4002–4006. [[CrossRef](#)]
30. Kim, H.; Lee, J.T.; Lee, D.C.; Magasinski, A.; Cho, W.I.; Yushin, G. Plasma-Enhanced Atomic Layer Deposition of Ultrathin Oxide Coatings for Stabilized Lithium–Sulfur Batteries. *Adv. Energy Mater.* **2013**, *3*, 1308–1315. [[CrossRef](#)]
31. Yu, M.; Yuan, W.; Li, C.; Hong, J.-D.; Shi, G. Performance Enhancement of a Graphene–Sulfur Composite as a Lithium–Sulfur Battery Electrode by Coating with an Ultrathin Al<sub>2</sub>O<sub>3</sub> Film Via Atomic Layer Deposition. *J. Mater. Chem. A* **2014**, *2*, 7360–7366. [[CrossRef](#)]
32. Meng, X.; Liu, Y.; Cao, Y.; Ren, Y.; Lu, W.; Elam, J.W. High-Performance High-Loading Lithium–Sulfur Batteries by Low Temperature Atomic Layer Deposition of Aluminum Oxide on Nanophase S Cathodes. *Adv. Mater. Interfaces* **2017**, *4*, 1700096. [[CrossRef](#)]
33. Harrison, K.L.; Zavadil, K.R.; Hahn, N.T.; Meng, X.; Elam, J.W.; Leenheer, A.; Zhang, J.-G.; Jungjohann, K.L. Lithium Self-Discharge and Its Prevention: Direct Visualization through in Situ Electrochemical Scanning Transmission Electron Microscopy. *ACS Nano* **2017**, *11*, 11194–11205. [[CrossRef](#)]
34. Kazyak, E.; Wood, K.N.; Dasgupta, N.P. Improved Cycle Life and Stability of Lithium Metal Anodes through Ultrathin Atomic Layer Deposition Surface Treatments. *Chem. Mater.* **2015**, *27*, 6457–6462. [[CrossRef](#)]
35. Kresse, G.; Furthmüller, J. Efficient Iterative Schemes for Ab Initio Total-Energy Calculations Using a Plane-Wave Basis Set. *Phys. Rev. B* **1996**, *54*, 11169–11186. [[CrossRef](#)]
36. Kresse, G.; Furthmüller, J. Efficiency of Ab-Initio Total Energy Calculations for Metals and Semiconductors Using a Plane-Wave Basis Set. *Comput. Mater. Sci.* **1996**, *6*, 15–50. [[CrossRef](#)]
37. Blöchl, P.E. Projector Augmented-Wave Method. *Phys. Rev. B* **1994**, *50*, 17953. [[CrossRef](#)] [[PubMed](#)]
38. Perdew, J.P.; Burke, K.; Ernzerhof, M. Generalized Gradient Approximation Made Simple. *Phys. Rev. Lett.* **1996**, *77*, 3865. [[CrossRef](#)]
39. Grimme, S.; Antony, J.; Ehrlich, S.; Krieg, H. A Consistent and Accurate Ab Initio Parametrization of Density Functional Dispersion Correction (Dft-D) for the 94 Elements H-Pu. *J. Chem. Phys.* **2010**, *132*, 154104. [[CrossRef](#)] [[PubMed](#)]
40. Guo, Q.; Lau, K.C.; Pandey, R. Thermodynamic and Mechanical Stability of Crystalline Phases of Li<sub>2</sub>S<sub>2</sub>. *J. Phys. Chem. C* **2019**, *123*, 4674–4681. [[CrossRef](#)]
41. Chen, L.; Connell, J.G.; Nie, A.; Huang, Z.; Zavadil, K.R.; Klavetter, K.C.; Yuan, Y.; Sharifi-Asl, S.; Shahbazian-Yassar, R.; Libera, J.A. Lithium Metal Protected by Atomic Layer Deposition Metal Oxide for High Performance Anodes. *J. Mater. Chem. A* **2017**, *5*, 12297–12309. [[CrossRef](#)]
42. Fan, Z.; Ding, B.; Zhang, T.; Lin, Q.; Malgras, V.; Wang, J.; Dou, H.; Zhang, X.; Yamauchi, Y. Solid/Solid Interfacial Architecturing of Solid Polymer Electrolyte–Based All-Solid-State Lithium–Sulfur Batteries by Atomic Layer Deposition. *Small* **2019**, *15*, 1903952. [[CrossRef](#)] [[PubMed](#)]
43. Lu, J.; Lei, Y.; Lau, K.C.; Luo, X.; Du, P.; Wen, J.; Assary, R.S.; Das, U.; Miller, D.J.; Elam, J.W. A Nanostructured Cathode Architecture for Low Charge Overpotential in Lithium-Oxygen Batteries. *Nat. Commun.* **2013**, *4*, 2383. [[CrossRef](#)] [[PubMed](#)]
44. Wang, H.; Dong, J.; Guo, Q.; Xu, W.; Zhang, H.; Lau, K.C.; Wei, Y.; Hu, J.; Zhai, D.; Kang, F. Highly Stable Potassium Metal Batteries Enabled by Regulating Surface Chemistry in Ether Electrolyte. *Energy Storage Mater.* **2021**, *42*, 526–532. [[CrossRef](#)]
45. Momma, K.; Izumi, F. VESTA 3 for Three-Dimensional Visualization of Crystal, Volumetric and Morphology Data. *J. Appl. Crystallogr.* **2011**, *44*, 1272–1276. [[CrossRef](#)]
46. Chen, Y.; Lu, S.; Zhou, J.; Wu, X.; Qin, W.; Ogoke, O.; Wu, G. 3d Graphene Framework Supported Li<sub>2</sub>S Coated with Ultra-Thin Al<sub>2</sub>O<sub>3</sub> Films: Binder-Free Cathodes for High-Performance Lithium Sulfur Batteries. *J. Mater. Chem. A* **2017**, *5*, 102–112. [[CrossRef](#)]
47. Galvez-Aranda, D.E.; Seminario, J.M. Li-Metal Anode in Dilute Electrolyte Lifs/Temp: Electrochemical Stability Using Ab Initio Molecular Dynamics. *J. Phys. Chem. C* **2020**, *124*, 21919–21934. [[CrossRef](#)]
48. Guo, Q.; Lau, K.C.; Pandey, R. Implication of Mechanical Properties of Li-S Binary Compounds Obtained from the First-Principles Study. *J. Phys. Chem. C* **2021**, *125*, 290–294. [[CrossRef](#)]